Mineralogical Magazine, April 2010, Vol. 74(2), pp. 257–268

Arisite-(La), a new *REE*-fluorcarbonate mineral from the Aris phonolite (Namibia), with descriptions of the crystal structures of arisite-(La) and arisite-(Ce)

P. C. Piilonen[1,*], A. M. McDonald[2], J. D. Grice[1], M. A. Cooper[3], U. Kolitsch[4], R. Rowe[1], R. A. Gault[1] and G. Poirier[1]

[1] Research Division, Canadian Museum of Nature, Ottawa, Ontario K1P 6P, Canada
[2] Department of Earth Sciences, Laurentian University, Sudbury, Ontario P3E 2C6, Canada
[3] Department of Geological Sciences, University of Manitoba, Winnipeg, Manitoba R3T 2N2, Canada
[4] Mineralogisch-Petrographische Abt., Naturhistorisches Museum, Burgring 7, A-1010 Wien, Austria

[*Received 14 January 2010; Accepted 14 April 2010*]

ABSTRACT

Arisite-(La), ideally $NaLa_2(CO_3)_2[F_{2x}(CO_3)_{1-x}]F$, is a new layered *REE*-fluorcarbonate mineral from miarolitic cavities within the Aris phonolite, Namibia (IMA no. 2009-019). It occurs as distinct chemical zones mixed with its Ce-analogue, arisite-(Ce). Crystals are vitreous, transparent beige, beige-yellow, light lemon-yellow to pinkish, and occur as tabular prisms up to 1.5 mm. Arisite-(La) is brittle, has conchoidal fracture, poor cleavage perpendicular to (001), a Mohs hardness of ~3−3½, is not fluorescent in either long- or shortwave UV radiation, dissolves slowly in dilute HCl at room temperature and sinks in methylene iodide, $D_{calc.}$ = 4.072 g cm^{-3}. Arisite-(La) is uniaxial negative, has sharp extinction, with both ω and ε exhibiting a range of values within each grain: ω = 1.696−1.717(4) and ε = 1.594−1.611(3), a result of chemical zoning attributed to both Ce ⇌ La and Na ⇌ Ca substitutions. The crystal structure of both arisite-(Ce) and arisite-(La) were solved by direct methods and refined to R = 1.66%, wR^2 = 4.31% (Ce) and R = 2.09%, wR^2 = 5.26% (La), respectively. Arisite is hexagonal, $P\bar{6}m2$, Z = 1, with unit-cell parameters of a = 5.1109(2) Å, c = 8.6713(4) Å, V = 196.16(6) Å^3 for arisite-(Ce), and a = 5.1131(7) Å, c = 8.6759(17) Å, V = 196.43(5) Å^3 for arisite-(La). Arisite-(Ce) and arisite-(La) are members of the layered, flat-lying *REE*-fluorcarbonate group which have crystal structures characterized by separate layers of triangular planar CO_3^{2-} groups that parallel the overall layering of the structure, F, *REE* and alkali or alkaline-earth elements. Overall, the arisite structure can be defined by three distinct layers which parallel (001): (1) $\infty[REE(CO_3)_2F]$ slabs, (2) sheets of $Na\phi_9$ polyhedra, and (3) $\infty[2F/CO_3]^{2-}$. Based on its (M+F)/C ratio, arisite can further be described as having a dense, flat-lying fluorcarbonate structure, a classification which includes the structurally related mineral species cordylite, kukharenkoite, cebaite, lukechangite, huanghoite, and one incompletely characterized synthetic phase, $NaY_2(CO_3)_3F$.

Keywords: fluorcarbonate, *REE*, Aris phonolite, structure determination, new mineral species.

Introduction

There are 25 known fluorcarbonate mineral species, 19 of which contain essential concentrations of rare-earth elements (*REE*) in their structure. The majority are the product of late-stage, often hydrothermal, crystallization in alkaline rock complexes including carbonatites, phonolites, nepheline syenites and their associated pegmatites, with a minor presence in granitic rocks. They are commonly associated with other carbonates, bicarbonates or *REE*-carbonates, fluorides, phosphates and silicates. Rare-earth

* E-mail: ppiilonen@mus-nature.ca
DOI: 10.1180/minmag.2010.074.2.257

fluorcarbonate minerals, in particular bastnäsite, provide the majority of the world's supply of *REE*. One major deposit, the Bayan Obo carbonatite in Inner Mongolia, north-central China, provides much of the world's requirements. Rare-earth fluorcarbonate minerals have a growing economic potential as their unusual optical and magnetic properties are important for industrial applications such as catalysis, permanent magnets, glass and ceramic manufacture, phosphors, lasers, bubble magnetic memories, and solid-oxide fuel-cell (SOFC) electrodes and electrolytes. As a result, synthesis of *REE*-fluorcarbonate species has become increasingly important, both for industry and for providing suitable material for mineralogical studies of natural mineral species which do not yield suitable crystals for crystal-structure analysis (Mercier and Leblanc, 1993*a*,*b*,*c*; Grice *et al.*, 2007). Many of these synthetic compounds have natural equivalents, yet many do not. Synthesis studies allow us to investigate further the conditions under which these unusual minerals crystallize.

Arisite-(La), and its Ce-analogue, arisite-(Ce) (Piilonen *et al.*, 2010) are two naturally occurring mineral species which, as of yet, do not have a stable synthetic equivalent. Arisite-(La) was discovered in phonolite from the Aris quarry, Namibia, and is named for its type locality. Both the mineral and the name have been approved by the IMA CNMMN (IMA no. 2009-019). Type material has been deposited at the Canadian Museum of Nature, Ottawa (CMNMC 86076).

Occurrence

The Aris phonolite in Namibia is part of the late Tertiary (33±1 Ma, Fitch and Miller, 1984) Auas alkaline volcanic province, which extends 65 km from Windhoek in the north to Rehoboth in the south. This volcanic province represents the most recent occurrence of alkaline magmatism along the western margins of southern Africa, similar to the Klinghardt Mountain alkaline volcanic province further to the south (37 Ma, Kröner, 1973; Marsh, 1987). The Auas alkaline volcanic province intrudes metasedimentary rocks (quartz-feldspar gneiss, mica schist and amphibolite) of the Paleoproterozoic Hohewarte complex. Gevers (1934) identified over 100 occurrences of both intrusive and extrusive alkaline rocks including trachyte, phonolite, shonkinite, alkali peridotite, and also a variety of tuffs, agglomerates and breccias. The phonolite and trachyte rocks occur as dykes and plugs which are exposed as eroded outcrops and caps on elevated hills and buttes. The Aris phonolite dyke occurs in the southern part of the province and is currently being mined for road and building material at the Ariskop and Railroad quarries. The phonolite is fine- to medium-grained, with an aphyric texture, and is composed predominantly of sanidine, nepheline and aegirine, with accessory haüyne, leucite, monazite and zircon (von Knorring and Franke, 1987**).** It also contains numerous miarolitic cavities that range from 0.1 mm to 10 cm in diameter, many of which are 'wet', containing residual hydrothermal formational fluids which are released when the cavities are broken open. Preliminary X-ray computed tomography at the University of Texas (Austin) indicates that 15–20% of the phonolite is comprised of miarolitic cavities. In some samples, 80% of these cavities are two-phase fluid + vapour-filled vugs. The miarolitic cavities host a range of agpaitic mineral species, including abundant villiaumite, aegirine, labuntsovite-group minerals, tuperssuatsiaite, natrolite, analcime, manganoneptunite, apophyllite-(KF), fluorite, and makatite. The presence of ubiquitous villiaumite in the cavities suggests a H_2O-poor environment. An extensive list of the known minerals within the Aris quarries has been given by Sturla *et al.* (2005). A detailed study of the mineralogy and paragenesis of these miarolitic cavities is ongoing.

Physical and optical properties

Arisite-(La) is visually indistinguishable from its Ce analogue, arisite-(Ce) (Piilonen *et al.*, 2010). It is brittle, has conchoidal fracture, poor cleavage parallel to (001), a Mohs hardness of ~3–3½, is non-fluorescent under either long- or short-wave UV radiation, and dissolves slowly with effervescence in dilute HCl at room temperature. Arisite-(La) sinks in methylene iodide (i.e. D >3.3 g cm^{-3}) and has a $D_{calc.}$ of 4.072 g cm^{-3}, $Z = 1$. Arisite-(La) occurs as euhedral, hexagonal plates up to 1.5 mm (average: 0.2 mm × 1.0 mm) and rare tabular, hexagonal prisms, in miarolitic cavities. The crystals are vitreous, transparent, and range in colour from beige, beige-yellow, light lemon-yellow to light pink. There is often a heavily included zone between the core and rim which imparts a clouded appearance to the crystals. Crystals are zoned, with arisite-(La)

cores and arisite-(Ce) rims, with additional minor Ca ⇌ Na substitution between core and rim. Chemical zoning is gradational from core to rim, with infrequent patchy, mottled zones. Not all crystals at Aris are zoned, and arisite-(Ce) is the dominant species. Observed forms include a dominant {001} pinacoid, with a minor {100} prism. Re-entrant angles have been noted on thicker crystals, but the twin law is not known. Arisite-(La) is uniaxial negative, has sharp extinction, with both ω and ε exhibiting a range of values within each grain: ω = 1.696−1.717(4) and ε = 1.594−1.611(3), a result of chemical zoning attributed to both Ce ⇌ La and Na ⇌ Ca substitutions. Associated minerals include aegirine, analcime, apatite, fluorite, manganoneptunite, microcline, natrolite, sphalerite, tupersuatsiaite, the unnamed, Fe-analogue of zakharovite, and arisite-(Ce). Arisite is a late-stage mineral which forms in miarolitic cavities in the phonolite, a result of crystallization from residual magmatic or hydrothermal fluids. It may be pseudomorphed to fine-grained, yellowish bastnäsite, resulting in opaque, dull crystals.

Chemical composition

Chemical analyses of arisite-(La) were carried out on a JEOL 733 electron microprobe operating in wavelength-dispersive mode, using the Geller Microanalytical system and programs. The operating conditions were as follows: operating potential 15 kV; probe current of 10 nA for Na, Ca and F, and 20 nA for the other elements; and final beam diameter of 20 μm. Data reduction was performed using a PAP routine in *XMAQNT* (C. Davidson, CSIRO, pers. comm.). A total of 14 elements were sought and the following X-ray lines and standards were employed during the analyses: Na (*K*α, albite), Ca (*K*α, calcite), Sr (*L*α, celestine), La (*L*α, synthetic $LaPO_4$), Ce (*L*α, synthetic $CePO_4$), Pr (*L*β, synthetic $PrPO_4$), Nd (*L*α, synthetic $NdPO_4$), Sm (*L*α, synthetic $SmPO_4$), Eu (*L*α, synthetic $EuPO_4$), Gd (*L*α, synthetic $GdPO_4$), Tb (*L*α, synthetic $TbPO_4$), Dy (*L*β, synthetic $DyPO_4$), Ho (*L*β, synthetic $HoPO_4$), and F (*K*α, CaF_2). Given the difficulties in analysing F by EMPA methods, and the importance of F in the arisite structure, additional steps were taken to ensure precise and accurate F measurements. Fluorine was measured using a TAP crystal and a fluorite standard (*K*α). The shape of the F *K*α peak was compared using slow WDS scans on standard and sample to ensure the suitability of the fluorite standard. Count times for all elements were 25 s, or shorter if a precision of 0.5% had already been attained, with 25 s count times for the background. Table 1 contains EMPA data for arisite-(La) and arisite-(Ce) from Aris, Namibia.

In order to determine the carbon content of arisite, crystals were analysed by laser-ablation inductively coupled plasma mass spectrometry (LA-ICP-MS). Two arisite grains were analysed for ^{13}C (at.%) using a beam size of 80 μm, 60% power, 20.8 J cm^{-2} fluence and a 5 Hz laser pulse. A standard of natural bastnäsite-(Ce) (Madagascar) was also employed. The average number of counts (n = 5) obtained from the NAM crystals was 3895 s^{-1} and for the bastnäsite-(Ce) (n = 2), 4417 s^{-1}. This suggests that the total C concentration is less than that of bastnäsite-(Ce) (ideal concentration: 5.48 at.% C). Using the average number of counts given by the bastnäsite-(Ce) and the ideal concentration of C in bastnäsite-(Ce), the concentration of C in arisite was calculated to be 4.83 at.%. It should be noted that the estimated error is ±1 at.%. LA-ICP-MS was also employed to check for the presence of B, which had values ranging from 8 to 11 ppm.

The empirical formula, calculated on the basis of seven negative charges, taking into consideration a $CO_3^{2-} \rightleftharpoons 2F^-$ substitution as determined from the single-crystal X-ray structure determination (see below), is $(Na_{0.99}Ca_{0.01})_{\Sigma 1.00}(La_{0.90}Ce_{0.83}Nd_{0.08}Pr_{0.03}Sm_{0.01}Ca_{0.14})_{\Sigma 1.99}(CO_3)_2[F_{0.73}(CO_3)_{0.63}]F$, with an ideal formula of $NaLa_2(CO_3)_2[F_{2x}(CO_3)_{1-x}]F$, which, for x = 1, requires Na_2O 6.49 wt.%, La_2O_3 68.19, CO_2 18.42, F 11.93, less O≡F 5.02, totalling 100.00 wt.%.

Powder X-ray diffraction

Powder X-ray diffraction data for arisite-(La) were collected with a Bruker AXS D8 Discover microdiffractometer using a Hi-Star area detector operated with a *GADDS* system, Cu-*K*α radiation (λ = 1.5418 Å) at 40 kV and 40 mA, with a sample-to-detector distance of 12 cm. The instrument was calibrated with synthetic corundum (PDF 00-10−0173) following a statistical calibration procedure (Rowe, 2009). Unit-cell refinement of the measured powder pattern was obtained by indexing the diffraction maxima using intensities from a powder pattern calculated using the program *Powdercell* (Nolze and Kraus, 1998). The refined unit-cell parameters are a =

TABLE 1. Electron microprobe (WDS) analyses for arisite-(La) and arisite-(Ce).

	Arisite-(La)					– Arisite-(Ce)† –	
Sample	NAM-1	NAM-2	NAM-3	NAM-4	NAM-Ave	NAM-Ave	MSH-Ave
Oxide (wt.%)							
La_2O_3	28.57	28.8	29.07	28.89	28.83	25.47	15.56
Ce_2O_3	27.87	26.09	26.25	27.22	26.86	29.8	30.71
Pr_2O_3	0.97	1.05	0.97	1.41	1.10	1.43	3.05
Nd_2O_3	2.82	2.49	2.47	2.95	2.68	3.54	8.12
Sm_2O_3	0.26	0.43	0.35	0.30	0.34	0.47	0.69
Eu_2O_3	b.d.	b.d.	b.d.	b.d.	b.d	0	0.07
Gd_2O_3	b.d.	b.d.	b.d.	b.d.	b.d	0	0.54
CaO	1.92	1.70	1.70	1.17	1.62	1.51	5.39
SrO	0.04	0.12	0.04	0.20	0.10	0.11	2.78
Na_2O	6.01	6.04	6.02	6.20	6.07	5.89	4.49
CO_2*	23.10	22.40	22.65	23.06	22.80	23.33	9.62
F	6.56	6.63	6.42	6.41	6.51	5.93	20.92
Sub total	98.12	95.75	95.94	97.81	96.91	97.48	101.33
Less O≡F	2.76	2.79	2.70	2.70	2.74	2.50	4.05
Total	95.36	92.96	93.24	95.11	94.17	94.98	97.28
Atoms per formula unit							
La	0.88	0.91	0.91	0.90	0.90	0.80	0.46
Ce	0.85	0.81	0.82	0.84	0.83	0.93	0.90
Pr	0.03	0.03	0.03	0.04	0.03	0.04	0.09
Nd	0.08	0.08	0.08	0.09	0.08	0.11	0.23
Sm	0.01	0.01	0.01	0.01	0.01	0.01	0.02
Eu	0.00	0.00	0.00	0.00	0.00	0.00	0.00
Gd	0.00	0.00	0.00	0.00	0.00	0.00	0.01
Ca	0.17	0.16	0.16	0.11	0.15	0.14	0.46
Sr	0.00	0.01	0.00	0.01	0.01	0.01	0.13
Na	0.97	1.00	1.00	1.01	0.99	0.97	0.70
F	1.73	1.79	1.73	1.70	1.74	1.59	2.43
CO_3	2.63	2.61	2.63	2.65	2.63	2.70	2.28

* calculated
b.d. below detection
† Piilonen *et al.* (2010)

5.1189(6) Å, c = 8.680(1) Å, V = 196.98(4) Å^3, Z = 1, and represent average values from zoned, locally La- or Ce-dominant crystals. The powder X-ray diffraction data are presented in Table 2.

Structure determination

Crystals of both arisite-(Ce) and arisite-(La) from Aris, Namibia, were selected for single-crystal X-ray diffraction studies on the basis of optical homogeneity and after initial electron microprobe analysis, used to confirm the dominance of Ce and La in the zoned crystals. Intensity data for both species were collected on a Bruker SMART system at the University of Manitoba consisting of a four-circle goniometer and a 4 K Apex CCD area-detector. Data were collected at room temperature using monochromatic Mo-$K\alpha$ radiation (50 kV, 40 mA), with a fixed detector-to-crystal distance of 5 cm. Frame widths of 0.2º ω and exposure times of 15 s were used. Data integration [2775 frames for arisite-(Ce) and 2766 frames for arisite-(La)] was done using the Bruker software *SAINT*, and absorption corrections were done using *SADABS* with crystals modelled as ellipsoids. Identical reflection data (at different ψ settings) were then merged using the program *XPREP* (Bruker, 1997) to give a total of 1538 reflections for arisite-(Ce) and 1557 for arisite-(La). Table 3*a* and 3*b* contain all information

TABLE 2. Powder X-ray diffraction data for arisite-(La).

$I_{obs.}$ NAM*	$d_{obs.}$ (Å) NAM	$I_{calc.}$**	$d_{calc.}$ (Å)**	*hkl*
100	**4.439**	**100**	**4.4281**	**100**
52	**4.352**	**37**	**4.3380**	**002**
10	3.950	6	3.9441	101
87	**3.103**	**77**	**3.0988**	**102**
38	**2.561**	**44**	**2.5566**	**110**
21	2.424	24	2.4213	103
43	**2.212**	33	2.2140	**200**
		26	**2.2025**	**112**
12	2.171	12	2.1689	004
42	**1.9748**	**52**	**1.9720**	**202**
16	1.9501	19	1.9478	104
12	1.9169	11	1.9154	113
3	1.7597	3	1.7580	203
10	1.6764	15	1.6737	210
11	1.6547	16	1.6539	114
7	1.6171	10	1.6156	105
13	1.5640	20	1.5615	212
7	1.5515	10	1.5494	204
3	1.4776	7	1.4760	300
3	1.4500	7	1.4486	213
		4	1.4357	115
4	1.3985	6	1.3974	302
3	1.3753	4	1.3746	106
1	1.3659	1	1.3657	205
5	1.3260	12	1.3250	214
		3	1.3147	303
3	1.2792	10	1.2783	220
		2	1.2586	116
4	1.2287	7	1.2281	310
		6	1.2262	222
		7	1.2203	304
2	1.2058	10	1.2046	215
2	1.1941	7	1.1935	107
4	1.1830	12	1.1817	312
1	1.1159	7	1.1153	117
2	1.0709	10	1.0726	402
		10	1.0687	314

* Intensities visually estimated. No internal standard was used and the film was corrected for shrinkage.
** As calculated from the refined crystal structure.

relevant to data collection and crystal structure determination.

The *Oscail* system (McArdle, 2004) which implements the *SHELX-97* package of programs (Sheldrick, 1997) was used for the solution and refinement of the crystal structure. Phasing of a set of normalized structure factors gave mean $|E^2-1|$ values of 0.586 for arisite-(Ce) and 0.551 for arisite-La (predicted values: 0.968 for centrosymmetric and 0.736 for non-centrosymmetric), low values, originally considered to be the result of merohedral twinning. Space group $P3$ was originally selected on the basis of the small calculated combined figure of merit. The structure was solved by Patterson methods and refined in space group $P3$ with scattering curves taken from Cromer and Mann (1968) and Cromer and Liberman (1970). An *E*-map was produced using calculated phase-normalized factors which allowed one Ce (La) and two oxygen atoms to be located. The structure was further refined on the basis of F^2 for all unique data. The remaining cation (Na^+, C^{4+}) and anion (O^{2-}, F^-) positions were located using difference Fourier maps during the refinement process. At this point, the program *MISSYM* (Lepage, 1988) was employed to search for higher symmetry and revealed the presence of additional symmetry elements, suggesting the actual space group to be $P\bar{6}m2$. The structure of arisite was transformed to this higher symmetry and refinement continued. The low *E*-statistics are thought to be the result of the presence of heavy Ce and La atoms on special positions within the structure.

It became apparent during the refinement process that there was a distinct discrepancy between the CO_3^{2-} and F^- contents determined (calculated) by EMPA and LA-ICP-MS and those determined from the structure refinement. Specifically: (1) LA-ICP-MS results indicated only 5 at.% C, corresponding to ~2 C a.p.f.u., whereas results from the structure refinement with two C sites indicated 3 C a.p.f.u.; (2) EMPA analyses indicated between 1.5 and 2.5 F a.p.f.u., whereas only one F was located in the structure refinement. Analyses of F by EMPA were performed a minimum of four times, and on two separate electron microprobes, to ensure that the values obtained were accurate. In the structure refinement, the site labelled 'C2' and originally thought to be a CO_3^{2-} group, was found: (1) to be partially occupied [(arisite-(Ce): 84%; arisite-(La): 94%)]; (2) to possess longer bond lengths than those generally observed for C–O bonds (~1.35 Å); and (3) to have anisotropic displacement factors which suggested smearing and disorder within the (001) plane. It is therefore considered that this site, subsequently labelled $\phi(2)$, is a mixed anionic site, containing a disordered array of both CO_3^{2-} and F^-. Assuming a mixed site, it was possible to relate

TABLE 3*a*. Crystal structure data for arisite-(Ce).

Space group	$P\bar{6}m2$		
a (Å)	5.1109(2)	Diffractometer	Bruker SMART system
c (Å)	8.6713(4)	Radiation	Mo-$K\alpha$ (50 kV, 40 mA)
V (Å^3)	196.16(6)	Crystal shape	Tabular
Z	1	Crystal size	$0.35 \times 0.29 \times 0.15$ mm^3
$\|E^2-1\|$	0.586	μ (Mo-$K\alpha$)	1.156 mm^{-1}
Min/max indices		$-7 \leqslant h \leqslant 3$, $-6 \leqslant k \leqslant 7$, $-11 \leqslant l \leqslant 12$	
Total reflections collected	1557		
Unique reflections	270		
$F_o > 4\sigma(F_o)$	270		
$R_{int.}$	0.0197		
GoF	1.472		
R_1	0.0166		
wR_2	0.0431		

Table 3*b*. Crystal structure data for arisite-(La).

Space group	$P\bar{6}m2$		
a (Å)	5.1131(7)	Diffractometer	Bruker SMART system
c (Å)	8.6759(17)	Radiation	Mo-$K\alpha$(50 kV, 40 mA)
V (Å^3)	196.43(5)	Crystal shape	Tabular
Z	1	Crystal size	$0.40 \times 0.29 \times 0.15$ mm^3
$\|E^2-1\|$	0.551	μ (Mo-$K\alpha$)	1.083 mm^{-1}
Min/max indices		$-6 \leqslant h \leqslant 7$, $-7 \leqslant k \leqslant 5$, $-10 \leqslant l \leqslant 12$	
Total reflections collected	1538		
Unique reflections	270		
$F_o > 4\sigma(F_o)$	270		
$R_{int.}$	0.0211		
GoF	1.763		
R_1	0.0209		
wR_2	0.0526		

$R_1 = \Sigma(|F_o|-|F_c|)/\Sigma|F_o|$
$wR_2 = [\Sigma(w)F_o^2-F_c^2)^2/\Sigma[w(F_o^2)^2]^{1/2}$, $w = 1/\sigma^2(F_o)$

the EMPA data to the structure refinement and achieve an acceptable answer.

The final structure of arisite-(Ce) was refined to R_1 = 1.66% and wR_2 = 4.31% with anisotropic displacement factors for all atoms except the mixed CO_3^{2-}/F^- site which was left isotropic. The structure of arisite-(La) was refined to R_1 = 2.09% and wR_2 = 5.26%. Table 4 contains the final positional and equivalent isotropic- and anisotropic displacement parameters. Table 5 contains selected interatomic distances for both species. Table 6*a*,*b* contains bond-valence sums for each species. Observed and calculated structure-factors are available at www.minersoc.org/pages/e_journals/dep_mat_mm.htm

Description of the structure

Arisite-(Ce) and arisite-(La) are isostructural layered *REE* fluorcarbonates with flat-lying CO_3^{2-} groups (Fig. 1). Arisite is hexagonal, $P\bar{6}m2$, Z = 1, with unit-cell parameters of a = 5.1109(2) Å, c = 8.6713(4) Å, V = 196.16(6) Å^3 for arisite-(Ce), and a = 5.1131(7) Å, c = 8.6759(17) Å, V = 196.43(5) Å^3 for arisite-(La). The structure of arisite contains two large metal

TABLE 4. Atomic coordinates and isotropic displacement factors ($Å^2 \times 10^3$) for arisite-(Ce) and arisite-(La).

Atom	*x*	*y*	*z*	U_{eq}
Arisite-(Ce)				
Na	0	0	0	13(1)
Ce	⅔	⅓	0.72542(4)	12(1)
C(1)	⅓	⅔	0.805(1)	13(2)
ϕ(2)	0	0	½	33(7)
O(1)	0.625(1)	0.8126(8)	0.8013(4)	17(2)
O(2)	0.8475(9)	0.1525(9)	½	26(2)
F	⅔	⅓	0	31(2)
Arisite-(La)				
Na	0	0	0	14(1)
La	⅔	⅓	0.72574(5)	11(1)
C(1)	⅓	⅔	0.804(1)	12(2)
ϕ(2)	0	0	½	44(10)
O(1)	0.627(3)	0.814(1)	0.8013(5)	19(2)
O(2)	0.847(1)	0.153(1)	½	25(2)
F	⅔	⅓	0	32(2)

cation sites (Na and *REE*), each with a distinct coordination polyhedron, one fully occupied flat-lying carbonate group, $C(1)O_3$, one fully occupied F^- site, and a mixed anionic site occupied by both CO_3^{2-} and F^-, ϕ(2), where ϕ = unspecified anion or anionic group. The crystal structures of both minerals are defined by $C(1)O_3$ carbonate groups oriented with their planar surface perpendicular to [001] (Fig. 1), with C(1)−O(1) = 1.292 Å and 1.302 Å for arisite-(Ce) and arisite-(La) respectively. The $^{[9]}$Na−ϕ polyhedron can be described as a regular trigonal prism, defined by six pinacoidal $O(1)^{2-}$ atoms [three above and below; with <Na−O(1)> = 2.392 Å for arisite-(Ce), and 2.387 Å for arisite-(La)] and three equatorial F^- [Na−F = 2.951 Å and 2.952 Å for arisite-(Ce) and arisite-(La), respectively], with an average <Na−ϕ> = 2.578 Å and 2.575 Å for arisite-(Ce) and arisite-(La) respectively. The $Naϕ_9$ polyhedra share corners *via* equatorial F atoms, resulting in Na−ϕ sheets within the (001) plane, and share edges with the $C(1)O_3$ carbonate group *via*

TABLE 5. Selected bond lengths (Å) for arisite-(Ce) and arisite-(La).

Arisite-(Ce)	Å	Arisite-(La)	Å
$^{[10]}$Ce−ϕ		$^{[10]}$La−ϕ	
Ce−F	2.3810(4)	La−F	2.3795(7)
Ce−O(2) ×3	2.526(5)	La−O(2) ×3	2.528(6)
Ce−O(1) ×6	2.645(1)	La−O(1) ×6	2.645(1)
<Ce−ϕ>	2.583	<Ce−ϕ>	2.583
$^{[9]}$Na−ϕ		$^{[9]}$Na−ϕ	
Na−O(1) ×6	2.392(6)	Na−O(1) ×6	2.387(9)
Na−ϕ ×3	2.9508(1)	Na−ϕ ×3	2.9520(4)
<Na−ϕ>	2.578	<Na−ϕ>	2.575
$^{[3]}$C(1−O(1) ×3	1.292(7)	$^{[3]}$C(1)−O(1) ×3	1.302(11)
$^{[3]}$C(2)−O(2) ×3	1.350(8)	$^{[3]}$C(2)−O(2) ×3	1.353(10)

TABLE 6*a*. Empirical bond valences (v.u.)* for arisite-(Ce).

	Ce	Na	C(1)	ϕ(2)	ΣV_a
O(1)	$0.263^{\times 6\rightarrow}_{\downarrow\ \times 2}$	$0.202^{\times 6}_{\downarrow}$	$1.303^{\times 3}_{\downarrow}$		2.031
O(2)	$0.363^{\times 3\rightarrow}_{\downarrow\ \times 2}$			$1.114^{\times 3}_{\downarrow}$	1.840
F	$0.360^{\rightarrow}_{\times 2}$	$0.032^{\times 3}_{\downarrow}$			0.816
ΣV_c	3.027	1.308	3.909	3.342	

Table 6*b*. Empirical bond valences (v.u.) for arisite-(La).

	La	Na	C(1)	ϕ(2)	ΣV_a
O(1)	$0.278^{\times 6\rightarrow}_{\downarrow\ \times 2}$	$0.205^{\times 6}_{\downarrow}$	$1.269^{\times 3}_{\downarrow}$		2.030
O(2)	$0.382^{\times 3\rightarrow}_{\downarrow\ \times 2}$			$1.105^{\times 3}_{\downarrow}$	1.869
F	$0.418^{\rightarrow}_{\times 2}$	$0.032^{\times 3}_{\downarrow}$			0.932
ΣV_c	3.232	1.326	3.807	3.315	

* Parameters from Brese and O'Keefe (1991).

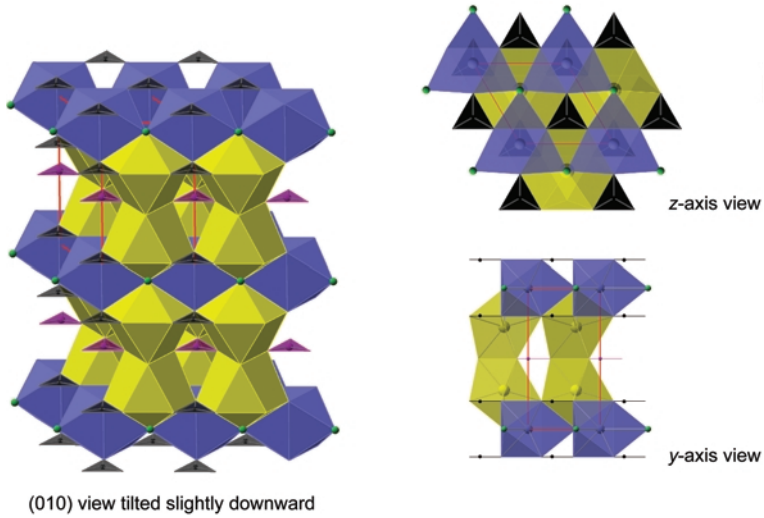

FIG. 1. The crystal structure of arisite: golden polyhedron = *REE*ϕ_{10}; blue polyhedron = Naϕ_9; black triangles = CO_3^{2-}; magenta triangles = mixed $[2F/CO_3]^{2-}$ site C(2) in a plane at z = ½; green spheres = F. The layered structure consists of three main components: (1) sheets of Naϕ_9 polyhedra, (2) ∞[*REE*$(CO_3)_2$F] slabs, and (3) $\infty[2F/CO_3]^{2-}$. The unit cell is outlined in red. The *REE*-ϕ_1 polyhedron is a monocapped hexagonal dipyramid, with nine O atoms defining a truncated end of the dipyramid and the F atom as the apex. The [*REE*O_9F] polyhedra share edges along the [001] axis, forming [*REE*O_6F] dimers which are further are linked along [001] *via* a bridging F. Naϕ_9 polyhedra share corners *via* their equatorial F, resulting in Na-F sheets within the (001) plane.

pinacoidal $O(1)^{2-}$ atoms at the top and bottom of the polyhedron. Only arisite-(Ce) from Mont Saint-Hilaire, Québec (Piilonen *et al.*, 2010) shows any appreciable Na ⇌ Ca substitution in this site (up to 0.30 a.p.f.u.). The $^{[10]}REE-\phi$ polyhedron can be described as a monocapped hexagonal dipyramid, with six O(1) and three O(2) atoms defining a truncated end of the dipyramid (<Ce−O> = 2.605 Å, <La−O> = 2.606 Å), and the F atom as the apex [Ce−F = 2.3810(4) Å; La−F = 2.3795(7) Å]. The site contains mainly Ce and La, with appreciable concentrations of Nd (up to 0.23 a.p.f.u.) and Pr (up to 0.09 a.p.f.u.). Each [REEO$_9$F] polyhedron shares an edge with an adjacent [REEO$_9$F] polyhedron along the [001] axis, forming [REEO$_6$F] dimers which are further linked along [001] *via* a bridging F^-. Pinacoidal $O(1)^{2-}$ anions link the $^{[10]}REE$-centred polyhedron to $C(1)O_3$ groups within the (001) plane, resulting in ∞[REE(CO$_3$)$_2$F] slabs. The mixed anionic site, $\phi(2)$, contains disordered CO_3^{2-} and F^-, thought to be a result of the F-rich/H_2O-poor environment (evidenced by the presence of ubiquitous villiaumite within the Aris phonolite miarolitic cavities). The $\phi(2)-O(2)$ bond lengths in this 'site' are ~1.35 Å, longer than expected for a C−O bond. The O(2) anion has a low bond-valence sum (BVS) of 1.87 v.u. In order for charge-balance considerations to be met, the overall structure can be defined by three distinct layers which parallel (001): (1) ∞[REE(CO$_3$)$_2$F] slabs; (2) sheets of Naϕ_9 polyhedra; and (3) $\infty[2F/CO_3]^{2-}$.

Discussion

Grice *et al*. (2007) recognized that previous attempts at developing a unified structural classification of fluorcarbonates did not take into consideration the effect of interaction of cations with two different anions, CO_3^{2-} and F^-. In response, they have presented a structural hierarchy of fluorcarbonates based on: (1) the fraction of cation, F^- and CO_3^{2-} [(M+F/C) where M = metal cation, F = fluorine, and $C = CO_3^{2-}$]; (2) the orientation of the CO_3^{2-} group relative to structure layering; (3) the arrangement of CO_3^{2-} groups relative to the crystallographic axes and relative to each other; (4) layer-layer substitutions; and (5) the coordination and complexing of F. Arisite-(Ce) and arisite-(La) are members of the layered, flat-lying *REE* fluorcarbonate group. These minerals all have crystal structures that are characterized by separate layers of triangular planar CO_3^{2-} groups

TABLE 7. Arisite and related *REE* fluorcarbonates.

Mineral	Formula	Space group	Cell dimensions							(M+F)/C	F/C
			a (Å)	b (Å)	c (Å)	α (°)	β (°)	γ (°)	Z		
Cordylite-(Ce)[1]	$(Na_{0.8}Ca_{0.1})BaCe_2(CO_3)_4F$	$P6_3/mmc$	5.1011(4)		23.096(4)	90	90	120	2	1.2	0.25
Cordylite-(Ce)[1]	$(Na_{0.44}Ca_{0.35})Ba(Ce_{1.85}Sr_{0.15})(CO_3)_4F$	$P6_3/mmc$	5.109(1)		23.289(9)				2	1.2	0.25
Cebaite-(Ce)[2]	$Ba_3Ce_2(CO_3)_5F_2$	$C2/m$	21.42(5)	5.087(5)	13.30(5)		94.8(2)		4	1.4	0.4
Huanghoite-(Ce)[3]	$BaCe_2(CO_3)_2F$	$R3c$	5.072(2)		38.46(1)	90	90	120	6	1.5	0.5
Lukechangite-(Ce)[4]	$Na_3Ce_2(CO_3)_4F$	$P6_3/mmc$	5.0612(8)		22.820(1)	90	90	120	2	1.5	0.25
Kukharenkoite-(Ce)[5]	$Ba_2Ce(CO_3)_3F$	$P2_1/m$	13.374(3)	5.1011(8)	6.653(1)		106.56(1)		2	1.3	0.33
Arisite-(Ce)	$NaCe_2(CO_3)_2[(CO_3)_{1-x}F_{2x}]F$	$Pm2$	5.1109(2)		8.6713(4)	90	90	120	1	1.8	0.59*
Arisite-(La)	$NaLa_2(CO_3)_2[F_{2x}(CO_3)_{1-x}]F$	$Pm2$	5.1131(7)		8.6759(17)				1	1.8	0.66*

[1] Giester *et al.* (1998), [2] Yang (1995), [3] Yang and Pertlik (1993), [4] Grice and Chao (1997), [5] Krivovichev *et al.* (1998).
* calculated from average EMPA analyses.

that parallel the overall layering of the structure, combined with composite layers of *REE* and alkali or alkaline-earth elements. This type of layering is very common in both natural and synthetic carbonate minerals and will dominate the fluorcarbonate structure when the proportion of CO_3^{2-}/F^- anions is large and the proportion of large cations to carbonate groups is approximately equal (Grice *et al.*, 2007). The *c*-cell dimensions of minerals in this 'flat-lying' group are based on multiples of the basic flat-lying $CaCO_3$ slab which has a thickness of ~2.85 Å. For example, aragonite has two slabs (c = 5.72 Å), calcite has six slabs (c = 17.06 Å), lukechangite-(Ce) eight slabs (c = 22.82 Å), cordylite-(Ce) eight slabs (c = 23.17 Å), and huanghoite-(Ce) twelve slabs (c = 38.46 Å). The *c*-cell dimension of arisite (c = 8.67 Å) suggests that, ideally three slabs should be present in the structure, as expressed in the hypothetical end-member $Na(REE)_2(CO_3)_2(CO_3)F$. In reality, the arisite solid solution possesses a mixed anionic interlayer site containing F^- and CO_3^{2-}, but which maintains the ideal slab *c*-dimension spacing.

The number of CO_3^{2-} groups within the unit cell allows us to classify fluorcarbonates further into dense [two complete CO_3^{2-} groups; $1.2 \leqslant (M+F)/C \leqslant 1.5$], open [one complete CO_3^{2-}, $3 \leqslant (M+F)/C \leqslant 4$], and lacunar [single, incomplete CO_3^{2-}, $(M+F)/C \geqslant 4$; Grice *et al.*, 2007]. Two possible hypothetical end members exist for the arisite solid solution structure, $NaREE_2(CO_3)_2(CO_3)F$ and $Na(REE)_2(CO_3)_2F_2F$, with $2 \leqslant CO_3^{2-} \leqslant 3$ (see also discussion in Piilonen *et al.*, 2010). On this basis, the arisite structure contains a minimum of two complete CO_3^{2-} groups within its unit cell and can therefore be described as having a dense, flat-lying fluorcarbonate structure. There are only five structurally-related mineral species in this group: cordylite, kukharenkoite, cebaite, lukechangite, and huanghoite, in addition to one known, incompletely-characterized synthetic phase, $NaY_2(CO_3)_3F$ (Table 7). All six phases are related to each other by the presence of $\infty[REE(CO_3)_2F]$ slabs (Fig. 2). When calculating the $(M+F)/C$ ratio for arisite, only the hypothetical CO_3-dominant end member has a ratio (1.33) in line with other dense, flat-lying *REE* fluorcarbonates; the F-dominant end member has a ratio (3.00) similar to that observed for flat and open *REE* fluorcarbonate structures which exist only in synthetic forms (Grice *et al.*, 2007). However, using the average observed arisite structure, we obtain a $(M+F)/C$ ratio of 1.80,

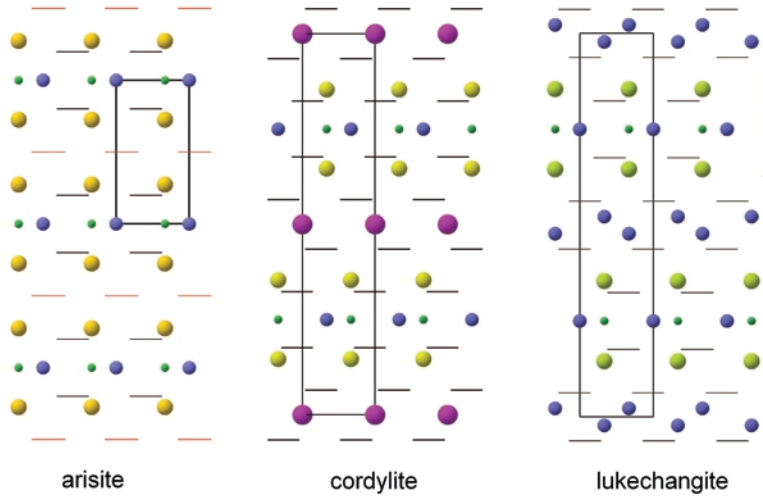

FIG. 2. The crystal structure of arisite and the related fluorcarbonate minerals cordylite-(Ce) and lukechangite-(Ce) viewed along the *y* axis. In the arisite structure there are sheets of $Na\phi_9$ polyhedra, $\infty[REE(CO_3)_2F]$ slabs and $\infty[2F/CO_3]^{2-}$. Note the presence of $\infty[REE(CO_3)_2F]$ slabs as the main building block in all three minerals. The unit cell is outlined, atoms as in the *y*-axis view shown in Fig. 1. Yellow spheres are *REE* (Ce). Blue spheres are Na in arisite and lukechangite-(Ce) and Na/Ca in cordylite-(Ce). Purple spheres in cordylite-(Ce) are Ba. Small green spheres are F in all structures. CO_3 groups lie parallel to (001) and are viewed on edge as black lines. In arisite, the mixed $[2F/CO_3]^{2-}$ site/triangle C(2) is seen on edge as a pink line.

slightly greater than that observed for other natural *REE* fluorcarbonates with dense, flat-lying structures [$1.2 \leqslant (M+F)/C \leqslant 1.5$]. The excess F in the arisite structure, as evidenced by the presence of a mixed CO_3^{2-}/F^- site, as compared to other dense, flat-lying *REE* fluorcarbonates, is the cause of this deviation from the normal range of $(M+F)/C$ observed ratios in natural minerals, and may reflect an evolution towards an intermediate structural configuration. Also of interest is the synthetic phase $NaY_2(CO_3)_3F$, observed in the system Na_2CO_3-YF_3-H_2O at 220ºC and for which crystals were grown at 500ºC, which contains $\infty[(REECO_3)(NaF)(REECO_3)]$ layers linked by $\infty(CO_3)^{2-}$ layers (Grice *et al.*, 2007; M. Leblanc pers. comm.). Although crystals of this phase are easily synthesized, the structure is, as of yet, undetermined, possibly due to the presence of disordered interlayer CO_3^{2-} groups and stacking faults. The difficulty in synthesizing this phase, and the presence of a disordered $\infty(CO_3)^{2-}$ may be related to the disorder that is observed in the arisite structure. At Aris, late-stage hydrothermal fluids were strongly enriched in F (and depleted in H_2O) as can be deduced from the mineralogy in the miarolitic cavities, i.e. the presence of ubiquitous villiaumite and fluorite. The high activity of F in the system during the final stages of crystallization may be responsible for the excess F in arisite, and thus the presence of a disordered $\infty[2F/CO_3]^{2-}$ layer. Further synthesis and single-crystal studies are required to elucidate this anomaly.

Acknowledgements

The authors thank mineral collectors, William Lechner, Andreas Palfi, Lázlo and Elsa Horváth, Robin Tibbit, Modris Baum, Markus Ecker, Stephan Wolfsried and Hans Vidar Ellingsen for providing the arisite-bearing material. Without their efforts, we would been unable to study these new species. Thanks are also extended to Prof. Frank C. Hawthorne, University of Manitoba, for use of the four-circle diffractometer. The comments and suggestions by Igor Pekov, Fernando Cámara, and an unknown reviewer were greatly appreciated. Research funding is provided by a RAC grant from the Canadian Museum of Nature (PCP), and NSERC (AMM).

References

Brese, N.E. and O'Keefe, M. (1991) Bond-valence parameters for solids. *Acta Crystallographica B*, **47**, 192–197.

Bruker (1997) *XPREP – Data preparation and Reciprocal Space Exploration*. Bruker AXS Inc., Madison, Wisconsin, USA.

Cromer, D.T. and Liberman, D. (1970) Relativistic calculation of anomalous scattering factors for X-rays. *Journal of Chemical Physics*, **53**, 1891–1898.

Cromer, D.T. and Mann, J.B. (1968) X-ray scattering factors computed from numerical Hartree-Fock wave functions. *Acta Crystallographica A*,, **24**, 321–324.

Fitch, F.J. and Miller, J.A. (1984) Dating Karoo igneous rocks by the conventional K-Ar and $^{40}Ar/^{39}Ar$ age spectrum methods. Pp. 247–266 in: *Petrogenesis of the Volcanic Rocks of the Karoo Province* (J.A. Erlank, editor). Special Publication **13**, Geological Survey of South Africa.

Gevers, T.W. (1934) Alkali-rocks in the Auas Mountains, south of Windhoek, S.W.A. *Transactions of the Geological Society of South Africa*, **36**, 77–88.

Giester, G., Ni., Y., Jarosch, D., Hughes, J.M., Rønsbo, J., Yang, Z. and Zemann, J. (1998) Cordylite-(Ce) A crystal chemical investigation of material from four localities, including type material. *American Mineralogist*, **83**, 178–184.

Grice, J.D. and Chao, G.Y. (1997) Lukechangite-(Ce), a new rare-earth-fluorocarbonate mineral from Mont Saint-Hilaire, Quebec. *American Mineralogist*, **82**, 1255–1260.

Grice, J.D., Maisonneuve, V. and Leblanc, M. (2007) Natural and synthetic fluoride carbonates. *Chemical Reviews*, **107**, 114–132.

Krivovichev, S.V., Filatov, S.K. and Zaitsev, A.N. (1998) The crystal structure of kukharenkoite-(Ce), $Ba_2REE(CO_3)_3F$, and an interpretation based on cation-coordinated F tetrahedra. *The Canadian Mineralogist*, **36**, 809–815.

Kröner, A. (1973) Comments on 'Is the African Plate stationary'. *Nature, Physical Science*, **243**, 29–30.

LePage, Y. (1988) MISSYM1.1 – a flexible new release. *Journal of Applied Crystallography*, **21**, 983–984.

Marsh, J.S. (1987) Evolution of a strongly differentiated suite of phonolites from the Klinghardt Mountains, Namibia. *Lithos*, **20**, 41–58.

McArdle, P. (2004) *Oscail* X - Windows Software for Crystallography and Molecular Modelling. NUI Galway, Ireland.

Mercier, N. and Leblanc, M. (1993*a*) Crystal growth and structures of rare earth fluorocarbonates: I. Structures of $BaSm(CO_3)_2F$ and $Ba_3La_2(CO_3)_5F_2$: revision of the corresponding huanghoite and cebaite type structures. *European Journal of Solid State and Inorganic Chemistry*, **30**, 195–205.

Mercier, N. and Leblanc, M. (1993*b*) Crystal growth and

structures of rare earth fluorocarbonates: II. Structures of zhonghaucerite $Ba_2Ce(CO_3)F$. Correlations between huanghoite, cebaite and zhonghaucerite type structures. *European Journal of Solid State and Inorganic Chemistry*, **30**, 207–216.

Mercier, N. and Leblanc, M. (1993*c*) Existence of 3d transition metal fluorocarbonates: synthesis, characterization of $BaM(CO_3)F_2$ (M = Mn,Cu) and crystal structure of $BaCu(CO_3)F_2$. *European Journal of Solid State and Inorganic Chemistry*, **30**, 217–225.

Nolze, G. and Kraus, W. (1998) PowderCell 2.0 for Windows. *Powder Diffraction*, **13**, 256–259.

Piilonen, P.C., McDonald, A.M., Grice, J.D., Rowe, R., Gault, R.A., Poirier, G., Cooper, M.A., Kolitsch, U., Roberts, A.C., Lechner, W. and Palfi, A.G. (2010) Arisite-(Ce), a new rare-earth fluorcarbonate from the Aris phonolite (Namibia), Mont Saint-Hilaire and the Saint-Amable sill (Québec). *The Canadian Mineralogist*, (in press).

Rowe, R. (2009) New statistical calibration approach for Bruker AXS D8 Discover microdiffractometer with Hi-Star detector using GADDS software. *Powder Diffraction*, **24**, 263–271.

Sheldrick, G.M. (1997) *SHELX-97. Program for the refinement of crystal structures*. University of Göttingen, Germany.

Sturla, M., Yakovenchuk, V.N. and Bonacina, E. (2005) Aris, Namibia: Geo-paragenesi e minerali. *Micro*, 55–80 (in Italian).

von Knorring, O. and Franke, W. (1987) A preliminary note on the mineralogy and geochemistry of the Aris phonolite, SWA/Namibia. *Communications of the Geological Survey of South Africa/Namibia*, **3**, 61.

Yang, Z. (1995) Structure redetermination of natural cebaite-(Ce), $Ba_3Ce_2(CO_3)_5F_2$, *Neues Jahrbuch für Mineralogie Monatshefte*, 56–64.

Yang, Z. and Pertlik, F. (1993) Huanghoite-(Ce), $BaCe(CO_3)_2F$, from Khibina, Kola Peninsula, Russia: Redetermination of the crystal structure with a discussion on the space group symmetry. *Neues Jahrbuch für Mineralogie Monatshefte*, 163–171.